

A New Approach for One-step Synthesis of Perovskite:fullerene Bulk Heterojunction Using Surfactant Free Microemulsion in Slot Die Method

Hemant S. Tarkas, Swapnil R. Tak, Vinita V. Deo, Sagar A. More, Devashri P. Upasani, Sanjay S. Ghosh, Jaydeep V. Sali

Department of Physics, School of Physical Sciences, Kavayitri Bahinabai Chaudhari North Maharashtra University, Jalgaon (MH), India

(Received 03 July 2020; revised manuscript received 21 December 2020; published online 25 December 2020)

Organometallic halide perovskite based solar cells are considered as the foundation of future photovoltaic technology. In these types of solar cells, it has been emphasized that the bulk heterojunction active layer architecture may show superior performance than the bilayer active layer architecture due to the increase in the interfacial area by intermixing both donor and acceptor phases in the bulk heterojunction. Organometallic halide perovskite with suitable acceptor in bulk heterojunction architecture can be a promising active layer in perovskite solar cells. Conventionally, the perovskite and acceptor are mixed together in a single solvent before thin film formation. Though this offers a one-step synthesis way, limited solubility of perovskite and acceptor in single solvent puts major constraint on the formation of bulk heterojunction through one-step solution processable method. This paper describes a new way of one-step synthesis of bulk heterojunction using surfactant free microemulsion in slot die method, which removes the constraint of limited solubility of the two phases in a single solvent. Emulsion of DMSO (solvent for $\text{CH}_3\text{NH}_3\text{PbI}_3$) and cyclohexane (solvent for PCBM) stabilized with acetone was used for making perovskite:fullerene bulk heterojunction. Solvent evaporation dynamics has been simulated to get deeper understanding of emulsion solidification leading to bulk heterojunction formation. Structural and optical studies support the formation of bulk heterojunction for efficient charge separation at donor:acceptor interfaces. A perovskite solar cell employing this bulk heterojunction has also been reported.

Keywords: Surfactant free microemulsion, Slot die coating, Perovskite:fullerene bulk-heterojunction solar cell, Simulation of evaporation dynamics.

DOI: [10.21272/jnep.12\(6\).06014](https://doi.org/10.21272/jnep.12(6).06014)

PACS numbers: 81.05.ub, 88.40.jp

1. INTRODUCTION

Organometallic halide perovskite based solar cells are the foundation of future photovoltaic technology due to their attractive features like tunable structural, compositional and optical properties. Additionally, cheaper and solution processable perovskite material reduces production cost and offers the flexibility in selection of proper fabrication technique. Hence, it is a promising competitor to the commercially available silicon solar cells. From 2009 to 2018, the recorded, NREL certified, perovskite solar cell efficiency drastically improved from 4 % to 25.2 %.

Spin coating technique has been utilized very often for the fabrication of Bilayer Heterojunction (BiHJ) and Bulk Heterojunction (BHJ) active layer architecture perovskite solar cells with one-step, two-step or three-step spin coating approaches. However, large material wastage and small deposition area limit the applicability of the spin coating method at an industrial scale. Other solution deposition techniques are already being explored for the perovskite solar cell fabrication, including doctor blade coating, ultrasonic spray technique, brush painting, inkjet printing, screen printing, and slot die coating. Among the deposition techniques mentioned above, slot die coating is one of the most suitable techniques for material efficient, large-scale device fabrication. Recently Jueng-Eun Kim et al. illustrated the one-step fabrication of a planar perovskite solar cell using N_2 gas blowing and heating assisted slot die technique and reported power conversion efficiency (PCE) of around 12.7 % after inclusion of Bifluo-

OMeTAD HTL layer [1].

The BHJ active layer architecture may show superior performance than the BiHJ architecture due to the increase in the interfacial area by intermixing both donor and acceptor phases. However, rather than deposition technique, there is a challenging difficulty in the preparation of a single-blend solution of donor and acceptor due to solubility limits of these components in a single solvent. The first report on BHJ by Chang Liu et al. [2] illustrated fabrication of $\text{CH}_3\text{NH}_3\text{PbX}_3:\text{PC}_{61}\text{BM}$ BHJ perovskite solar cells by using the two-step solution-processed spin coating method. The obtained results validate the improved features of BHJ over BiHJ. Recently, Cong Liu et al. achieved 16.6 % PCE and 80 % fill factor for perovskite:F4TCNQ BHJ based solar cell device by applying the additive engineering strategy [3]. The inclusion of *p*-type Cu(Tu)I as the trap state passivation of perovskite in constructing the perovskite:Cu(Tu)I BHJ inverted device architecture showed very promising PCE of 19.9 % [4]. Chien-Hung Chiang et al. [5] have obtained the PCE of 12.1 % by mixing 0.1 wt. % PCBM (limited due to solubility limit) with PbI_2 in DMF solvent and MAI in isopropyl alcohol. The BHJ was deposited by using a two-step spin coating method. In the same report, they illustrated the necessity of extra PCBM layer over spin coated BHJ active layer for efficient charge transport and improved the PCE up to 16 %. In overall, preparing a single blend solution of the donor and acceptor is the challenge in fabrication of BHJ using a one-step method. Our group has proposed a solution to such a problem in the case of the formation on BHJ of a donor polymer (P3KHT) sol-

uble in water and an acceptor (PCBM) soluble in organic solvent, by using the concept of emulsion and demonstrated the formation of BHJ [6]. Here, based on a similar concept, we used a novel Surfactant-Free Micro-Emulsion (SFME) made of cyclohexane, acetone, and DMSO referred hereafter as CAD SFME for the fabrication of $\text{CH}_3\text{NH}_3\text{PbI}_3$ -PCBM BHJ solar cell using slot die technique. DMSO is a good solvent for $\text{CH}_3\text{NH}_3\text{PbI}_3$ and cyclohexane is a good solvent for PCBM. Moreover, both solvents are immiscible. An emulsion of DMSO and cyclohexane can be formed by mixing them with a specific amount of the third component acetone. This scheme avoids intimate pre-mixing of $\text{CH}_3\text{NH}_3\text{PbI}_3$ and PCBM and can lead to pure perovskite and PCBM phase formation during solidification. In this work, we also simulated the evaporation of the component solvents of the SFME to predict the behavior of the emulsion during solidification of the microemulsion resulting in the formation of BHJ. This work successfully demonstrates and opens a new way of formation of $\text{CH}_3\text{NH}_3\text{PbI}_3$ -PCBM BHJ using SFME in one-step deposition of an active layer using slot die method.

2. EXPERIMENTAL

The slot die setup used in this work is shown in Fig. 1. It includes a slot die nozzle made up of stainless steel with meniscus guide of a width of 10 mm. The gap between two dies was maintained by PTFE tape of about 125 μm thickness.

Air shroud was attached on the rear side of the nozzle 2.5 cm above the substrate surface. During deposition, airflow rate was maintained at 5 l/min using a precise gas flow controller. Solution was fed to the slot die head with 5 ml/h flow rate by using a syringe pump. Lip was maintained at 100 μm height from the substrate on a hot plate.

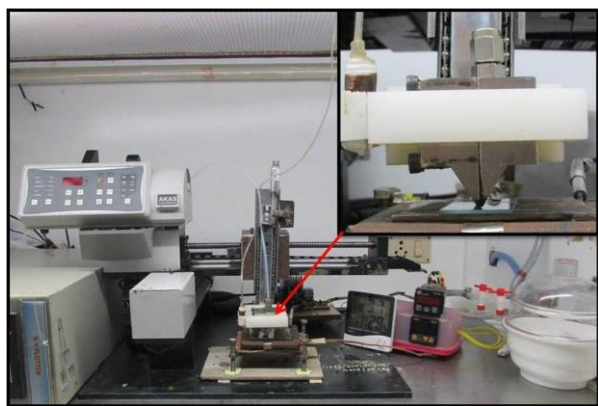


Fig. 1 – Experimental setup of slot die technique used in this work

2.1 Synthesis of Methylamine Iodide ($\text{CH}_3\text{NH}_3\text{I}$) MAI Powder

20 ml of hydroiodic acid (HI) (strong acid) was taken in an ice bath. 18.78 ml of equimolar methylamine (CH_3NH_2) (weak base) was then added dropwise in HI by using syringe pump at 120 ml/h solution flow rate with continuous stirring. The whole reaction was carried out in dark conditions. After two hours of continu-

ous stirring, the solution was kept in the vacuum oven at 100 $^\circ\text{C}$ for removing the solvent and to obtain a white powder of $\text{CH}_3\text{NH}_3\text{I}$.

2.2 Preparation of CAD SFME

First, PbI_2 powder was dissolved in CAD micro-emulsion by using ultrasonic bath sonication at 45 $^\circ\text{C}$. To adjust the MAI: PbI_2 ratio to 1:1, equimolar powder of $\text{CH}_3\text{NH}_3\text{I}$ was then added with continuous sonication to obtain low 0.125 M and high 0.2 M solution concentrations. High solution concentration value was determined by the solubility limit of solutes, especially PbI_2 , in the microemulsion. After 15 min sonication, we added acceptor PCBM with 0.5 wt. % and 1.0 wt. % in the two microemulsions with ultrasonication for making emulsion with two different acceptor concentrations.

2.3 Device Fabrication

The device architecture and energy level diagram for the fabricated perovskite BHJ solar cell are shown in Fig. 2a and Fig. 2b, respectively. FTO substrates were cleaned using soap solution, double distilled water, acetone and isopropyl alcohol with 5 min bath sonication successively. The cleaned FTO substrates were dried at 100 $^\circ\text{C}$ for 60 min. After drying, 50 nm thick, transparent and compact TiO_2 (c- TiO_2) layer was deposited using the 1.5 ml solution of titanium (IV) isopropoxide in 10 ml ethanol and 0.1 ml hydrochloric acid using spin coating method at 4000 rpm for 45 s. The films were dried at 125 $^\circ\text{C}$ for 15 min and then annealed at 500 $^\circ\text{C}$ for 30 min [7].

Followed by c- TiO_2 layer, a mesoporous TiO_2 (m- TiO_2) layer was deposited by using spin coating. Commercially available TiO_2 powder (Degussa P25), comprising ~ 20 nm sized TiO_2 nanoparticles, was preheated at 120 $^\circ\text{C}$ for 60 min to remove impure hydroxide phase. A paste was then prepared by dispersing 1.1 g of preheated TiO_2 powder in 8.5 ml ethanol and 1.5 ml acetyl acetone, using probe sonication at 220 Watt for 30 min. Acetyl-acetone acts as a dispersion-stabilizing agent. The temperature of the paste was controlled by preparing an ice bath during probe sonication to prevent preheating and evaporation of the solvent. This paste was then spin coated over c- TiO_2 coated FTO substrate at 4000 rpm for 45 s, and then dried at 125 $^\circ\text{C}$ for 10 min. Thickness of the layer was ~ 800 nm. After drying, the sample was sintered by transferring into muffle furnace at 500 $^\circ\text{C}$ temperature for 30 min.

Devices were fabricated in an open environment at laboratory conditions (room temperature 28 $^\circ\text{C}$ and relative humidity ~ 20 %) by using emulsions with perovskite concentration of 0.2 M with 1.0 wt. % PCBM. FTO/c- TiO_2 /m- TiO_2 deposited substrates were kept on a hot substrate holder. The CAD microemulsion was fed to the slot die nozzle using a syringe pump at 5 ml/h solution flow rate. The slot die head was moved over the substrate using programmable X-Y plotter with a speed of 1 mm/s. A dry air was showered over the deposited area with 5 l/min flow rate controlled by using precise gas flow controller. After deposition of BHJ active layers, the samples were transferred to a vacuum oven at 100 $^\circ\text{C}$ for 10 min post deposition thermal annealing.

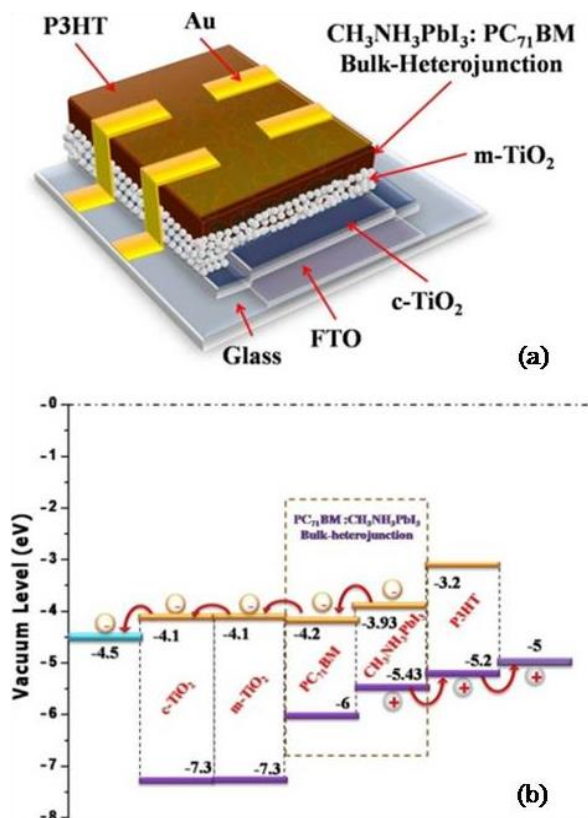


Fig. 2 – (a) Schematic diagram of the device fabricated in this study. Device architecture: FTO/c-TiO₂/m-TiO₂/CH₃NH₃PbI₃ PCBM/P3HT/Au; (b) energy level diagram for the device

A thin P3HT hole transport layer was then spin coated over CH₃NH₃PbI₃:PCBM BHJ active layer using 5 mg/ml solution of P3HT in *o*-dichlorobenzene at 4000 rpm for 60 s. The samples were annealed at 100 °C for 5 min. After annealing, all samples were shifted into the thermal evaporation system to deposit 70 nm thick gold (Au) electrodes at 10⁻⁶ mbar pressure.

3. RESULTS AND DISCUSSION

We found that with 0.25 M concentration of MAI and PbI₂, both solutes completely dissolved in the CAD microemulsion by prolonged sonication. Further increase in the concentration, however, resulted in the formation of residues of PbI₂ at the bottom of the CAD microemulsion containing beaker even after one hour of sonication at 50 °C. Based on this observation, 0.2 M was taken as the higher and 0.125 M as the lower concentration for the study. Substrate temperature and solution concentration are some of the important parameters governing the film formation process by slot die method. In the case of solution based thin film deposition techniques, it is essential to optimize the substrate temperature for developing a good quality film [8]. Importance of substrate temperature optimization in slot die method has been outlined by Tianshi Qin et al. [9] reporting their work on HTL deposited using slot die technique. Giovanni Cotella et al. [10] also highlighted the role of substrate temperature in perovskite crystal growth through controlling the solvent evaporation rate. The effect of substrate temperature on substrate coverage and crystallinity of perovskite thin

films by slot die method has also been reported by Kyeongil Hwang et al. [11]. On this background, substrate temperature for these two solution concentrations was optimized to get uniform, pinhole free and compact perovskite films on FTO/c-TiO₂/m-TiO₂ substrate. In this work, the films were formed at substrate temperature ranging from 70 °C to 90 °C with post deposition annealing at 100 °C for 15 min. Control on solvent evaporation rate is essential to get pinhole free perovskite film with good crystallinity.

The solvent evaporation rate of the deposited ink can be controlled either by heating the substrates or by introducing an airflow over the surface during the coating procedure. Giovanni Cotella et al. [10] used the substrate heated from 65 °C to 90 °C to promote rapid drying dynamics similar to the spinning process and generate a thermal gradient which promotes the crystal growth horizontally instead of vertically. However, they observed that higher temperatures gave poor surface coverage while the intermediate temperatures led to an increased surface coverage. Similar observations are recorded in this work.

The optical microscope images captured in transmission mode are shown in Fig. 3. Row [A]: CH₃NH₃PbI₃ (0.125 M) and row [B]: CH₃NH₃PbI₃ (0.2 M).

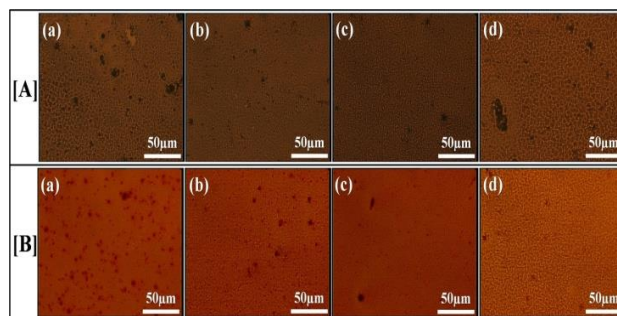


Fig. 3 – Optical microscope images (transmission mode) of CH₃NH₃PbI₃ thin films deposited on glass/FTO/c-TiO₂/m-TiO₂ substrate at a substrate temperature of a) 70 °C, b) 80 °C, c) 85 °C, and d) 90 °C; row [A]: CH₃NH₃PbI₃ (0.125 M) and row [B]: CH₃NH₃PbI₃ (0.2 M)

It was observed that the surface coverage improved as we increased the substrate temperature from 70 °C to 85 °C. However, with further increase in temperature to 90 °C, good surface coverage could not be achieved. Similar trend with respect to surface coverage is observed for both solution concentrations. Further, with an increase in the substrate temperature up to 85 °C the presence of pinholes was also observed to be decreased, which increased with an increase in the substrate temperature to 90 °C. Thus, a very specific substrate temperature is needed to control the solidification of perovskite thin films with good surface coverage and pinhole free morphology. Based on these observations, we choose 85 °C as the optimum value of the substrate temperature for deposition of CH₃NH₃PbI₃ thin films using CAD microemulsion. The average thickness of the film with solution concentration of 0.125 M was found to be ~ 180 nm and that of prepared with a solution concentration of 0.2 M was about ~ 400 nm.

We then studied the formation of perovskite:PCBM BHJ using perovskite and PCBM dissolved in CAD mi-

croemulsion. For this, 0.1 wt. % and 0.2 wt. % of PCBM was dissolved in each microemulsion with 0.125 M and 0.2 M perovskite concentrations. The films were deposited on FTO/c-TiO₂/m-TiO₂ substrate at a substrate temperature of 85 °C. The film formation process as decided by state of microemulsion during solidification is governed by evaporation dynamics of different solvents in the microemulsion. To understand this, we simulated the evaporation of the three solvents in the microemulsion system. The simulation was simplified with assumption that the evaporation rates of the solutions are equal to the evaporation rates of respective solvents in the microemulsion. We determined the evaporation rate of the pooling solvents at different temperatures by using the United States Air Force Method (USAFM) described by Robert D. Morrison [12].

The equation used for calculating the evaporation flux (E_r) is as below:

$$E_r = (4.161 \cdot 10^{-5}) \cdot u^{0.75} T_F M \left(\frac{P_s}{P_H}\right) \text{ g}/(\text{cm}^2 \cdot \text{s}), \quad (\text{a})$$

where u is the wind speed (m/s), T_F is the liquid temperature-correction factor, M is the pooled liquid molecular weight (g/mol), P_s is the pooled liquid vapor pressure at ambient temperature (mm Hg), and P_H is the vapor pressure of hydrazine at ambient temperature (mm Hg), T_P is the pooled liquid surface temperature (°C). If $T_P = 0$ °C or less, $T_F = 1.0$, otherwise $T_F = 1.0 + 0.0043 T_P^2$. The hydrazine vapor pressure (P_H) at absolute ambient temperature (T_A in K) is given as

$$P_H = 760 \cdot \exp\left[65.3319 - \left(\frac{7245.2}{T_A}\right) - (8.22 \cdot \ln T_A) + (6.1557 \cdot 10^{-3}) T_A\right]. \quad (\text{b})$$

During deposition, the substrate to slot die tip distance was fixed at 100 μm. Hence, it was assumed that the thickness (T_h) of the developed liquid film is ~ 100 μm. The total exposed area of the emulsion was assumed to be constant till complete solidification, because solidification of the liquid film starts from bottom to the top surface. We calculated the volume of different solvents evaporated as a function of time using the following relation:

$$\Delta V = (E_r/\rho) \cdot A \cdot \Delta t. \quad (1)$$

The exposed area of the three solvents as a function of time was also determined based on their relative volumes.

Fig. 4a shows variation in the volume of the three solvents as a function of time. The inset shows an expanded view of the initial time scale. Due to different evaporation rates, the proportion of cyclohexane and DMSO in the solidifying microemulsion goes on changing as a function of time. Accordingly, the quantity of acetone required to sustain microemulsion state also varies as a function of time. Fig. 4b shows variation of the quantity of acetone as a function of time during solidification and the amount of acetone required to sustain microemulsion state for that dynamic microemulsion composition. The results indicate that the evaporation dynamics of different solvents in microemulsion makes acetone insufficient to sustain the microemulsion state during very initial stage of solidification and the microemulsion becomes unstable. So, one may expect the formation of totally separated phase layers of perovskite

and PCBM after complete solidification of the solution.

However, observation of the HR-SEM images eliminates this possibility. The HR-SEM images of the substrate FTO/compact-TiO₂/mesoporous-TiO₂ as well as different layers on the substrate viz. perovskite, perovskite + 0.5 wt. % PCBM and perovskite + 1 wt. % PCBM for two different precursor concentrations for perovskite formation are shown in Fig. 5. The perovskite thin film formed with 0.2 M concentration shows a compact film with good substrate coverage compared to that formed with 0.125 M concentration. With 0.125 M concentration of perovskite, BHJ film formed with 0.5 wt. % of PCBM shows marginal presence of PCBM on the surface in the form of spherical structures.

Increase in wt. % of PCBM to 1 wt. % shows not many changes in the surface features of the film with 0.125 M precursor concentration. However, interesting features can be observed on the surface of BHJ films with 0.5 wt. % and 1 wt. % of PCBM in perovskite with 0.2 M solution concentration. From Fig. 4b, it can be seen that both cyclohexane (solvent for PCBM) and acetone (stabilizing agent for emulsion) are completely evaporated within first 500 ms. Thus, solidification of PCBM occurs within a few hundred milliseconds. However, it takes around 9.5 s for DMSO to evaporate completely and form solid perovskite phase. It seems that although the emulsion is de-stabilized during the initial stage of solvent evaporation, the total uniting of 'cyclohexane + PCBM' droplets is hindered by the presence of a perovskite solution, with high resistance in a high concentration perovskite compared to a low concentration perovskite. This results in the formation of channels of PCBM phase embedded in perovskite medium, as seen in Fig. 5. UV-Visible optical absorption spectra in Fig. 6 are also in agreement with the results obtained from the optical microscopic and HR-SEM results.

Pristine perovskite films formed with 0.125 M solution show less absorption values compared to those formed with 0.2 M solution. Strong absorption at 550 nm in films with 0.2 M precursor signifies better formation of perovskite crystals compared to that with 0.125 M solution. High precursor solution concentration is essential for better crystallization and consequently better light harvesting [13]. With addition of PCBM, in general, absorbance values and its range enhance. Similar results were obtained for both solution concentrations and PCBM wt. % but the values of the optical absorbance are different due to differences in film thicknesses.

Reduction in PCBM absorption below 400 nm is observed with 0.5 wt. % PCBM in a perovskite film with high concentration. A similar reduction of PCBM absorption has been noted for annealed blends of poly(3-hexylthiophene) (P3HT) with PCBM [14]. The effect is possibly related to enhanced long-range ordering in the neat PCBM regions [15]. Rise in PCBM absorption below 400 nm in films with 1 wt. % PCBM in 0.2 M perovskite suggests that PCBM uniting leading to a long-range ordering after breaking emulsion stability is hindered by an increase in PCBM loading in high concentration perovskite solution. In low concentration (0.125 M) perovskite solution, long-range ordering is not reflected in absorption spectra possibly due to less PCBM loading in the perovskite solution. X-ray diffrac-

tion patterns obtained for these films support these observations. The XRD patterns for these films along with the compact TiO₂ layer deposited using spin coating and mesoporous TiO₂ layer are shown in Fig. 7.

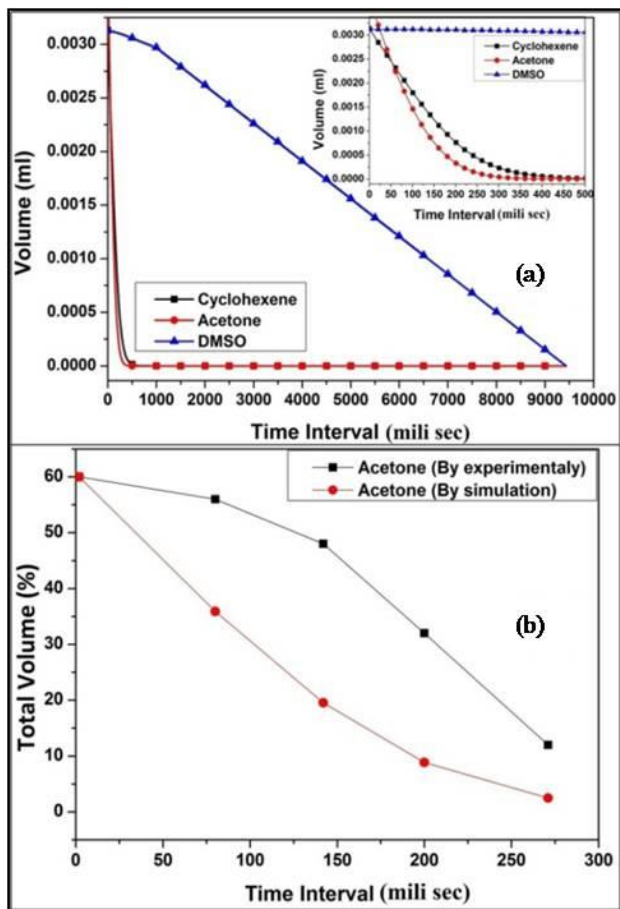


Fig. 4 – (a) Volume of component solvents of microemulsion as a function of time at 85 °C substrate temperature; (b) variation in amount of volume of acetone (in %) present in solidifying microemulsion as decided by simulation (circles), and that required to keep microemulsion stabilized as decided by experiments (squares) as a function of time

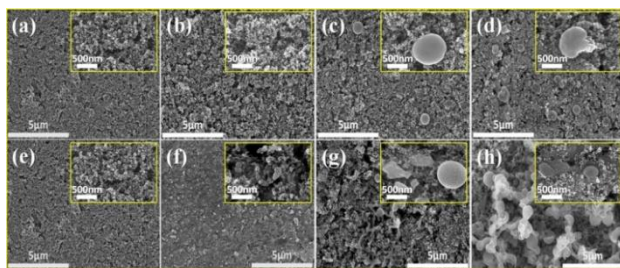


Fig. 5 – FE-SEM images of thin films (a) and (e) m-TiO₂ deposited over FTO/c-TiO₂ substrate; (b) CH₃NH₃PbI₃ film with 0.125 M solution concentration; (c) CH₃NH₃PbI₃ (0.125 M):PCBM (0.5 wt. %); (d) CH₃NH₃PbI₃ (0.125 M):PCBM (1.0 wt. %); (f) CH₃NH₃PbI₃ with 0.2 M solution concentration; (g) CH₃NH₃PbI₃ (0.2 M):PCBM (0.5 wt. %) and (h) CH₃NH₃PbI₃ (0.2 M):PCBM (1.0 wt. %)

The diffraction peak at 25.34° is associated with (101) plane. Anatase TiO₂ is known to be a suitable phase for the TCO applications in various optoelectronic devices because of the wide bandgap (3.2 eV), rela-

tively low effective mass of electron $\sim 1 m_0$ and high refractive index than ITO [16]. The m-TiO₂ scaffold layer enhances the charge collection via improved surface area as compared to only c-TiO₂ window layer.

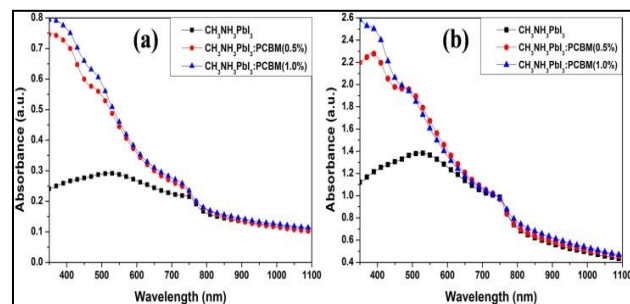


Fig. 6 – (a) Absorption spectra of CH₃NH₃PbI₃ and CH₃NH₃PbI₃:PCBM thin films deposited at 85 °C for 0.125 M perovskite solution concentration; (b) absorption spectra of CH₃NH₃PbI₃ and CH₃NH₃PbI₃:PCBM thin films deposited at 85 °C for 0.2 M perovskite solution concentration

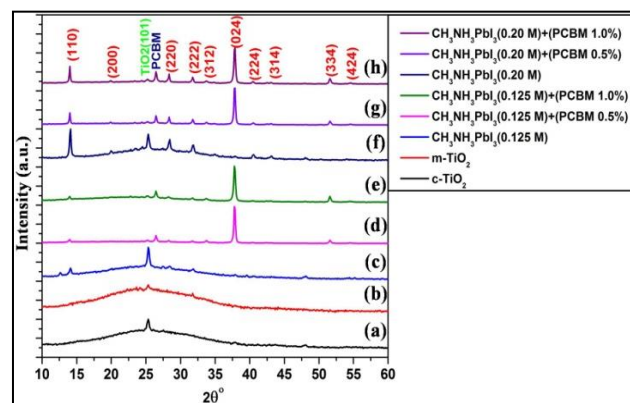


Fig. 7 – XRD patterns of (a) c-TiO₂, (b) m-TiO₂, (c) CH₃NH₃PbI₃, (d) CH₃NH₃PbI₃:PCBM (0.5 wt. %), (e) CH₃NH₃PbI₃:PCBM (1.0 wt. %) thin films deposited at 85 °C for 0.125 M solution concentration. XRD patterns of (f) CH₃NH₃PbI₃, (g) CH₃NH₃PbI₃:PCBM (0.5 wt. %) and (h) CH₃NH₃PbI₃:PCBM (1.0 wt. %) thin films deposited at 85 °C for 0.2 M solution concentration

Strong characteristic (110), (220) and (222) diffraction peaks of tetragonal perovskite phase at 14.11°, 28.51° and at 31.75° [17] are observed in XRD pattern of the films formed with higher concentration and not in films formed with lower concentration, probably due to insufficient perovskite deposition. One interesting feature is the change in preferred orientation of perovskite from (110) to (024) with addition of PCBM. Formation of tetragonal perovskite phase with preferred (024) orientation in thin films formed by spin-coating method has been reported by Binglong Lei et al. [17].

The films were excited with 740 nm for recording the steady-state PL spectra. It was observed that the PL emission from perovskite films deposited with higher concentration was much larger than the emission from films deposited at lower concentration. In case of perovskite thin films deposited with lower solution concentration (0.125 M), the pristine perovskite film showed suppressed luminescence compared to perovskite:PCBM thin films. A report by Ka Kan Wong et al. concluded that as TiO₂ does not form an ideal interface with MAPbI₃, this may lead to non-radiative recomb-

nation at the TiO_2 - MAPbI_3 interface [18]. Very thin deposition of perovskite phase, due to low solution concentration, results in less crystallinity and dominant interface effect compared to the bulk and this may be the cause of suppressed radiative luminescence in this perovskite film. Interestingly, when a small fraction (0.5 wt. %) of PCBM was added to perovskite, the PL emission increased. This observation can be attributed to increased crystallinity of perovskite in the presence of PCBM, leading to a decrease in non-radiative recombination centers. XRD patterns for these films support this view. XRD shows an increase in diffraction peak intensities for perovskite material in BHJ film as compared to pristine perovskite materials indicating an enhancement in crystallinity. When PCBM loading was increased to 1 wt. %, PL quenching effect due to charge separation at donor-acceptor interface was observed.

Steady-state PL spectra of pristine perovskite thin film deposited with 0.2 M solution and perovskite:PCBM BHJ thin films with different PCBM concentrations are shown in Fig. 8b. For perovskite:PCBM BHJ thin films with 0.5 wt. % of PCBM concentration, large PL quenching was observed without any peak shifting. Significant PL quenching indicates efficient charge separation at the donor:acceptor interface. Further increase in acceptor concentration to 1.0 wt. % showed almost similar PL quenching.

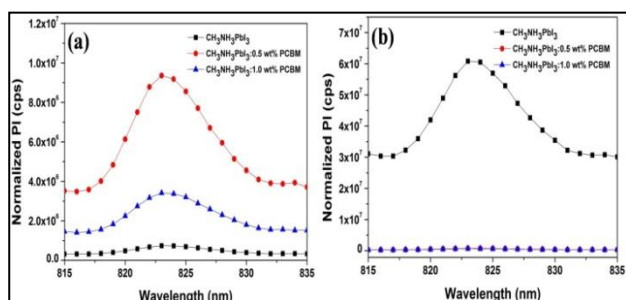


Fig. 8 – Steady-state PL spectra of (a) $\text{CH}_3\text{NH}_3\text{PbI}_3$ and $\text{CH}_3\text{NH}_3\text{PbI}_3$:PCBM (0.5 wt. %), $\text{CH}_3\text{NH}_3\text{PbI}_3$:PCBM (1.0 wt. %) thin films deposited at 85 °C with 0.125 M perovskite solution concentration; (b) $\text{CH}_3\text{NH}_3\text{PbI}_3$ and $\text{CH}_3\text{NH}_3\text{PbI}_3$:PCBM (0.5 wt. %), $\text{CH}_3\text{NH}_3\text{PbI}_3$:PCBM (1.0 wt. %) thin films deposited at 85 °C with 0.2 M perovskite solution concentration, respectively

Based on this study, for the comparison, we fabricated $2 \times 2 \text{ mm}^2$ sized perovskite solar cell devices, with the pristine perovskite and perovskite:fullerene BHJ based active layer. Additionally, we recorded the device performance with and without P3HT HTL layer also. A similar study with multiple repetitions of device fabrication showed that comparatively, FTO/c- TiO_2 /m- TiO_2 / $\text{CH}_3\text{NH}_3\text{PbI}_3$:PCBM/P3HT/Au device architecture gives better PV performance.

The concentration of perovskite solution was 0.2 M and 1 wt. % of PCBM was used in the emulsion. Dark and illuminated J - V characteristics of the better performing device are shown in Fig. 9.

The device performance (PCE = 0.4 %) is limited by low V_{oc} (0.35 V) as well as low values of FF (49 %) and current density (1.91 mA/cm^2). Presence of shortening paths, recombination centers at the interfaces and non-optimized active-layer and HTL thickness can be the reasons behind poor performance of the device. It has

been reported by Wenmei Ming et al. [19] that due to low formation energies and low diffusion barriers for Au^+ , Au can diffuse into MAPbI_3 from their respective electrodes even at room temperature.

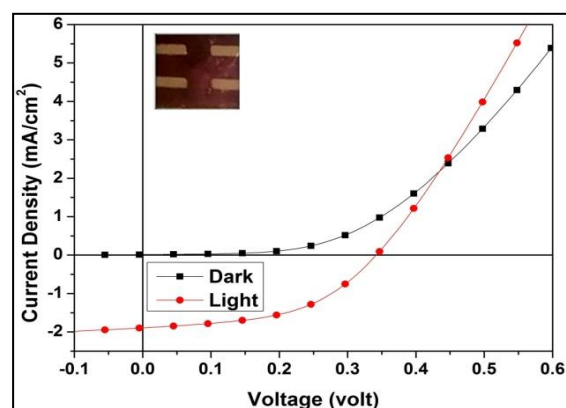


Fig. 9 – J - V characteristics of $\text{CH}_3\text{NH}_3\text{PbI}_3$:PCBM BHJ perovskite solar cell device fabricated using CAD solution deposited by slot die coating with P3HT HTL layer

In our case, Au diffusion into the active layer may be the reason for low I_{sc} and low shunt resistance (820Ω) of the device. In addition, Au diffusion under illumination is the second problem with Au contact.

Stefania Cacovich et al. [20] suggested that it is necessary to reduce this diffusion by employing alternative HTMs, replacing gold or working on interlayers. The illuminated J - V curve crosses the dark J - V curve in the first quadrant. This indicates reduction in collection of photogenerated current with an increase in forward bias. This can be due to the recombination at the interfaces. In this work, the moto behind device fabrication was just to prove the concept of BHJ active-layer fabrication by a novel route using microemulsion. More systematic work on the device fabrication can improve the device performance.

4. CONCLUSIONS

In conclusions, this article opens a new approach for one-step synthesis of perovskite:fullerene BHJ using surfactant free microemulsion in slot die method. BHJ of $\text{CH}_3\text{NH}_3\text{PbI}_3$:PCBM was successfully prepared using surfactant-free microemulsion of DMSO (solvent for $\text{CH}_3\text{NH}_3\text{PbI}_3$) and cyclohexane (solvent for PCBM) formed with acetone as the stabilizing agent. Although the simulation results indicate destabilization of microemulsion during initial steps of solidification, SEM images showed the formation of interpenetrating morphology of the two phases. Steady-state PL spectroscopy results confirmed efficient charge separation at the donor:acceptor interfaces. A working perovskite solar cell with BHJ prepared by this method as an active layer indicates potential to explore this route more deeply.

ACKNOWLEDGEMENTS

Hemant S. Tarkas acknowledges the financial support of the Department of Science and Technology, New Delhi under INSPIRE Fellowship Scheme. The work was also supported by UGC under SAP-Phase-II.

REFERENCES

1. J. Kim, Y. Jung, Y. Heo, K. Hwang, T. Qin, D. Kim, D. Vak, *Sol. Energy Mater Sol. C.* **179**, 80 (2018).
2. C. Liu, K. Wang, P. Du, C. Yi, T. Meng, X. Gong, *Adv. Energy Mater.* **5**, 1402024 (2015).
3. C. Liu, Z. Huang, X. Hu, X. Meng, L. Huang, J. Xiong, L. Tan, Y. Chen, *ACS Appl. Mater. Interface.* **10**, 1909 (2018).
4. S. Ye, H. Rao, Z. Zhao, L. Zhang, H. Bao, W. Sun, Y. Li, F. Gu, J. Wang, Z. Liu, Z. Bian, C. Haung, *J. Am. Chem. Soc.* **139**, 22 7504 (2017).
5. C. Chiang, C Wu, *Nat. Photon.* **10**, 196 (2016).
6. M. Mahajan, G. Lonkar, S. Ghosh, M. Patil, D. Dalal, J. Sali, *J. Phys. D: Appl. Phys.* **48**, 265105 (2015).
7. V. Eze, B. Lei, T. Mori, *Jpn. J. Appl. Phys.* **55**, 02BF08 (2016).
8. Y. Jung, K. Hwang, F. Scholes, S. Watkins, D. Kim, D. Vak, *Sci. Rep.* **6**, 20357 (2016).
9. T. Qin, W. Huang, J. Kim, D. Vak, C. Forsyth, C. McNeill, Y. Cheng, *Nano Energy* **31**, 210 (2017).
10. G. Cotella, J. Baker, D. Worsley, F. Rossi, P. Cameron, C. Matthew, T. Watson, *Sol. Energy Mater Sol. C.* **159**, 362 (2017).
11. K. Hwang, Y. Jung, Y. Heo, F. Scholes, S. Watkins, J Subbiah, D. Jones, D. Kim, D. Vak, *Adv. Mater.* **27**, 1241 (2015).
12. *Introduction to Environmental Forensics, Ed. 3* (R.D. Morrison) (Academic Press: Elsevier: 2015).
13. J. Im, I. Jang, N. Pellet, M. Grätzel, N. Park, *Nature Nanotechnology* **9**, 927 (2014).
14. M. Faist, P. Keivanidis, S. Foster, P. Wöbkenberg, T Anthopoulos, D. Bradley, J. Durrant, J. Nelson, *J. Polym. Sci., Part B: Polym. Phys.* **49**, 45 (2011).
15. M. Schmidt, A. Bruno, J. Yao, S. King, S. Tuladhar, T. Kirchartz, M. Alonso, A. Goñi, N. Stingelin, S. Haque, M. Campoy Quiles, J. Nelson, *Adv. Funct. Mater.* **24**, No. 44, 6972 (2014).
16. J. Yan, J Emilio, P. Juarez, G. Qianqing, *Mater. Horiz.* **3**, 548 (2016).
17. B. Lei, V. Eze, T. Mori, *Jpn. J. Appl. Phys.* **54**, 100305 (2015).
18. K. Wong, A. Fakhruddin, P. Ehrenreich, T. Deckert, M. Abdi-Jalebi, R. Friend, S. Lukas, *J. Phys. Chem. C* **122**, No 20, 10691 (2018).
19. W. Ming, D. Yang, T. Li, L. Zhang, M. Du, *Adv. Sci.* **5**, No 2, 1700662 (2017).
20. S. Cacovich, L. Cinà, F. Matteocci, G. Divitini, P. Midgley, A. Carlo, C. Ducati, *Nanoscale*, **9**, 4700 (2017).